INTERNATIONAL JOURNAL OF HYDROGEN ENERGY 37 (2012) 4633–4638

Available at www.sciencedirect.com

ScienceDirect

journal homepage: www.elsevier.com/locate/he

Carbon-coated tungsten oxide nanowires supported Pt nanoparticles for oxygen reduction

Madhu Sudan Saha [a,1], Yong Zhang [a], Mei Cai [b], Xueliang Sun [a,*]

[a] Department of Mechanical and Materials Engineering, The University of Western Ontario, London, Ontario N6A 5B9, Canada
[b] General Motors Research and Development Center, Warren, MI 48090-9055, USA

ARTICLE INFO

Article history:
Received 28 February 2011
Received in revised form
2 May 2011
Accepted 3 May 2011
Available online 11 June 2011

Keywords:
Carbon-coated tungsten oxide nanowires
Catalyst support
Polymer electrolyte membrane fuel cells
Pt nanoparticles
Oxygen reduction reaction

ABSTRACT

Carbon-coated tungsten oxide nanowires were grown directly on carbon fiber of a carbon paper (C–$W_{18}O_{49}$ NWs/carbon paper) by chemical vapor deposition method and Pt nanoparticles were deposited on the nanowires (Pt/C–$W_{18}O_{49}$ NWs/carbon paper) to form the composite electrode. The microstructure and electrochemical behavior of the resultant Pt/C–$W_{18}O_{49}$ NWs/carbon paper composites are characterized by a transmission electron microscope (TEM) and cyclic voltammetry, respectively. The electrocatalytic activities of these composite electrodes for oxygen reduction reaction (ORR) were investigated and higher mass and specific activities in ORR were exhibited as compared to commercial Pt/C electrode.

1. Introduction

Proton exchange membrane fuel cells (PEMFCs) have received considerable attention in recent years as alternative energy devices for transportation and portable power generation applications [1–3]. However, two main challenges limit the application of fuel cells in transport [4]: (i) the sluggish kinetics of the oxygen reduction reaction (ORR) on the cathode side which reduces the efficiency of PEMFCs; and (ii) the cost of the membranes and precious metal-based electrocatalysts is too high for mass production and marketing. In order to reduce cathode-activation losses due to the comparably sluggish kinetics of the oxygen reduction reaction, more active catalysts should be used [5,6]. One way to improve cathode performance is to use supported Pt catalysts that have higher surface area and lower platinum loading [7–9]. Further improvement, related to the reduction of the activation potential of the cathode and at the same time to lowering its price, can be achieved by using Pt-based alloys with transition metals. It has been reported that the alloying of Pt with non-precious-metals such as Co [10,11], Cr [12,13], Ni [10,12], Fe [14], Mn [15] and V [16] shows higher activity for the ORR than Pt-alone. The improvement in the ORR electrocatalysis has been ascribed to different factors such as a decrease in the Pt–Pt distance and therefore a more favorable adsorption of O_2 [11], the lowering of the Pt oxidation state [17], the suppression of Pt oxide formation [17,18], the formation of a new electronic structure with 5*d*-orbital vacancies [10,11] and the formation

* *Corresponding author*. Tel.: +1 519 661 2111x87759; fax: +1 519 661 3020.
E-mail addresses: mssaha@ymail.com (M.S. Saha), xsun@eng.uwo.ca (X. Sun).
[1] Present address: NRC Institute for Fuel Cell Innovation, 4250 Wesbrook Mall, Vancouver, British Columbia V6T 1W5, Canada.
0360-3199/$ – see front matter
doi:10.1016/j.ijhydene.2011.05.013

of a catalytic and thin Pt skin on the surface of the alloy [10,19,20].

The most widely used conventional support of the Pt catalysts is higher surface area carbon black (Vulcan XC-72). However, the carbon black is known to undergo electrochemical oxidation to surface oxides, and to CO_2 under fuel cell conditions [21]. As carbon corrodes, noble metal nanoparticles on carbon black will detach from the electrode or aggregate to larger particles resulting in Pt surface area loss, which subsequently lowers the performance of PEMFCs [22]. Therefore, many efforts have been made to search new catalyst supports [23].

Metal–metal oxide catalysts have been investigated as possible co-catalysts that are believed to operate via the bi-functional mechanism [24–26]. Specifically, tungsten oxide (WO_3) has been the subject of interest in this role and has been used as a support material for fuel cell catalysts [25,27–29]. It was reported that Pt nanoparticles supported on WO_3 catalysts exhibited excellent CO tolerance [29,30] and higher catalytic activity. According to Savadogo and Beck, the electrocatalytic activity of Pt/WO_3-based electrode toward the oxygen reduction reaction in phosphoric acid was twice as high as that of Pt on carbon [31].

One-dimensional nanostructures such as nanowires, nanobelts, nanotubes, and nano-cables have attracted remarkable attention because of their novel electric, magnetic, optical and mechanical properties and their wide range of potential applications in nano-devices [32]. In our previous studies, we proposed the idea of growing NWs directly on carbon paper (fuel cell backing) as catalyst support [33–35]. The unique advantage of this approach is that all the deposited catalyst particles are in electrical contact with the external electrical circuit and much improved Pt utilization has been achieved [33–35].

As a continuation of our interest on metal oxide nanowires as catalyst supports, we report here the growth of carbon-coated $W_{18}O_{49}$ NWs directly on carbon paper (C–$W_{18}O_{49}$ NWs/carbon paper). The Pt nanoparticles were deposited on the C–$W_{18}O_{49}$ NWs/carbon paper by the reduction of Pt precursor with glacial acetic acid. The Pt nanoparticles supported on the C–$W_{18}O_{49}$ NWs/carbon paper were characterized using TEM and the electrocatalytic activities of these composite electrodes for oxygen reduction reaction were investigated.

2. Experimental

2.1. Synthesis of carbon-coated $W_{18}O_{49}$ NWs

The synthesis of carbon-coated $W_{18}O_{49}$ NWs directly on carbon paper (C–$W_{18}O_{49}$ NWs/carbon paper) was carried out in a horizontal tube furnace as described previously [36]. Carbon paper with a layer of 450 nm thick W film was placed in the middle of the furnace. A carrier gas of high purity argon (99.999%) was passed through the quartz tube at a rate of 300 sccm (standard cubic centimeters per minute) through warm water bubbler. After 20 min, the furnace was heated up to 750 °C and kept at that temperature for 1 h. In the last 30 min of the experiment along with argon gas a carbon gas (C_2H_4) with a flow of 2–3 sccm was introduced into the chamber. Then the furnace was allowed to cool to room temperature in the flowing carrier gas.

2.2. Deposition of Pt nanoparticles on C–$W_{18}O_{49}$ NWs

Pt nanoparticles were deposited on the C–$W_{18}O_{49}$ NWs/carbon paper by the reduction of Pt precursors with glacial acetic acid as described previously [37]. In a typical procedure, required amount of Pt precursor was added into 25 ml of glacial acetic acid and it was agitated in an ultrasonic bath for 10 min. The C–$W_{18}O_{49}$ NWs/carbon paper was placed into the solution and maintained at a temperature of 110 ± 2 °C for around 5 h under constant stirring. Afterward, the Pt nanoparticles supported C–$W_{18}O_{49}$ NWs/carbon paper composites were washed with deionized water and dried at 85 °C over night in a vacuum oven.

2.3. Characterization

The morphologies of composites were characterized using a scanning electron microscope (SEM) (Hitachi S-2600 N) and transmission electron microscope (TEM) (Philips CM10). X-ray diffraction (XRD) analysis was also carried out with an X-ray diffractometer (Rigaku-MiniFlex) using Cu K_a radiation at 30 kV. The Pt loading in the Pt/C–$W_{18}O_{49}$ NWs/carbon paper composites was determined to be 0.18 mg/cm^2 by inductively coupled plasma-optical emission spectroscopy (ICP-OES).

Cyclic voltammetry (CV) was conducted at room temperature using an Autolab potentiostat/galvanostat (Model, PGSTAT-30, Eco Chemie, Brinkmann Instruments) with a three-electrode, two-compartment configuration. Pt wire and a reversible hydrogen electrode (RHE) were used as the counter and reference electrodes, respectively. Purified Ar (99.9998%) and O_2 (<99.5%) gases were purchased from Praxair Canada Inc. For comparison purpose, a conventional electrode made with commercially available 30 wt.% Pt/C obtained from E-TEK, USA was also evaluated by applying a catalyst layer composing Pt/C catalyst, Nafion solution and iso-propanol to the gas diffusion layer. The ratio of dry Nafion to Pt/C was 1:3 by weight and the Pt loading was 0.20 mg/cm^2 on the electrode. For the measurement of hydrogen electrosorption curves were measured in Ar-purged 0.5 M H_2SO_4 aqueous solution with the potential cycling between −0.0 and +1.2 V at a scan rate of 50 mV/s to obtain the voltammograms of hydrogen adsorption. The catalytic activities for oxygen reduction reaction were carried out in O_2-saturated 0.5 M H_2SO_4 solution. Note that the current was normalized to the mass of platinum.

3. Results and discussion

Fig. 1 shows the typical SEM and TEM images of C–$W_{18}O_{49}$ NWs grown on carbon fibers of carbon paper by thermal evaporation method. SEM image reveals the bulk yield growth of the nanowires on the carbon fibers as shown in Fig. 1(a). Further, TEM images reveal that the diameter of the nanowires is mostly ranging from 30 nm to 60 nm with a typical size of 50 nm as shown in Fig. 1(b) inset.

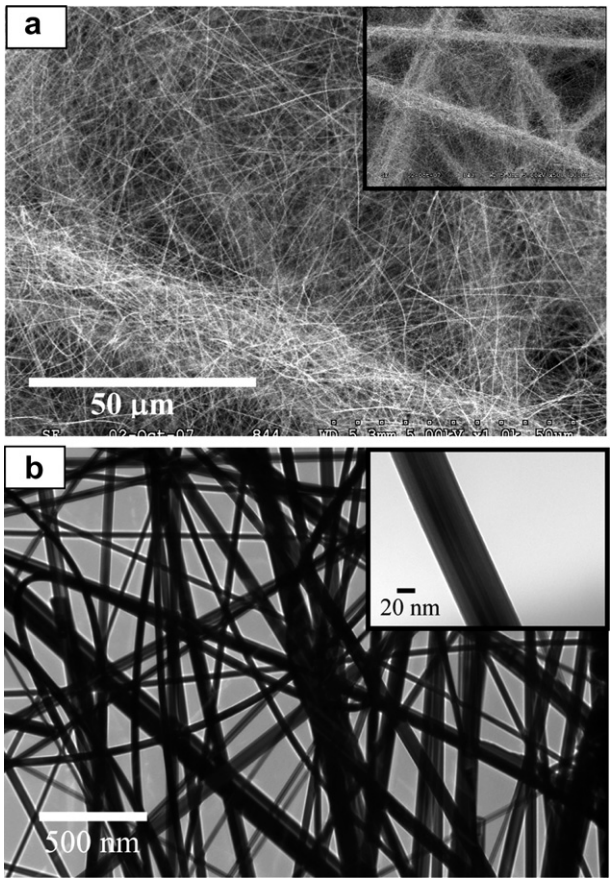

Fig. 1 – SEM and TEM images of C–$W_{18}O_{49}$ NWs grown on carbon fibers of carbon paper by thermal evaporation method. (a) SEM image showing full coverage of NWs on fibers of carbon paper. (Inset): Higher magnification. (b) TEM image showing individual C–$W_{18}O_{49}$ NWs. (Inset): Single NW.

To identify phase structure of the obtained C–$W_{18}O_{49}$ NWs, XRD of the nanowires was performed as shown in Fig. 2. The sharp diffraction peaks in Fig. 2 were identified as monoclinic $W_{18}O_{49}$ (JCPDS No. 05-0392). Further, the high relative intensity of the peak at $2\theta = 23.5°$ indicates oriented growth of the nanowires along the ⟨010⟩ crystal direction. On the other hand, no obvious tungsten peaks were observed, indicating that the reaction from tungsten to tungsten oxide was more complete because of the introduction of C_2H_4. Therefore, XRD analyses indicate that the resultant nanowires are composed of single-crystalline $W_{18}O_{49}$ NWs.

Fig. 3 shows typical TEM images of C–$W_{18}O_{49}$ NWs/carbon paper after deposition of Pt nanoparticles. It was clearly observed that Pt nanoparticles are distributed on the surface of NWs uniformly without large aggregation. The histogram of Pt particle size distribution obtained by measuring 300 randomly chosen particles in the magnified TEM images is shown in Fig. 3(c). It can be found that the Pt particles have a relatively narrow particle size distribution of 1–3 nm.

The electrosorption properties of Pt nanoparticles on C–$W_{18}O_{49}$ NWs/carbon paper composite were examined by CV shown in Fig. 4. For comparison, the commercial Pt/C

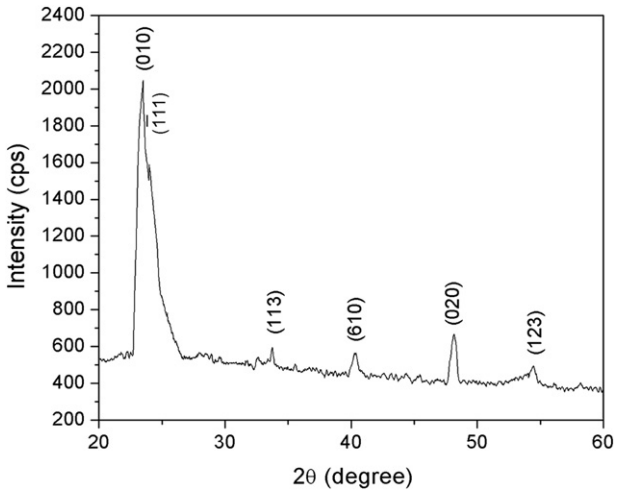

Fig. 2 – XRD pattern of C–$W_{18}O_{49}$ NWs grown directly on carbon paper.

electrocatalyst from E-TEK (30 wt.% Pt on carbon black) was also examined at the same conditions. The voltammetric features of both electrodes reveal the typical characteristics of Pt metal [38], with Pt oxide formation in the +0.8 to +1.2 V

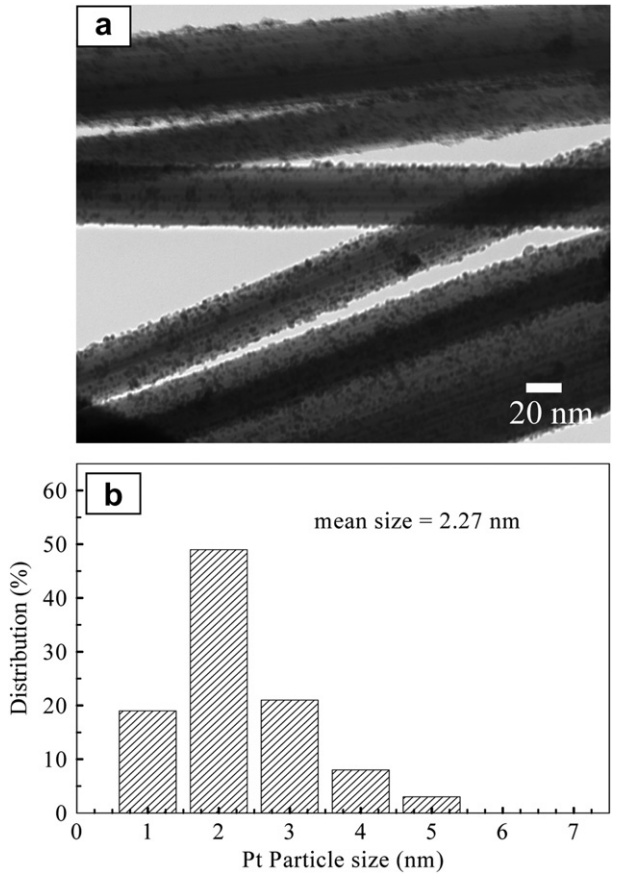

Fig. 3 – (a) TEM images of Pt nanoparticles deposited on the C–$W_{18}O_{49}$ NWs/carbon paper by glacial acetic acid method and (b) the corresponding particle size distribution.

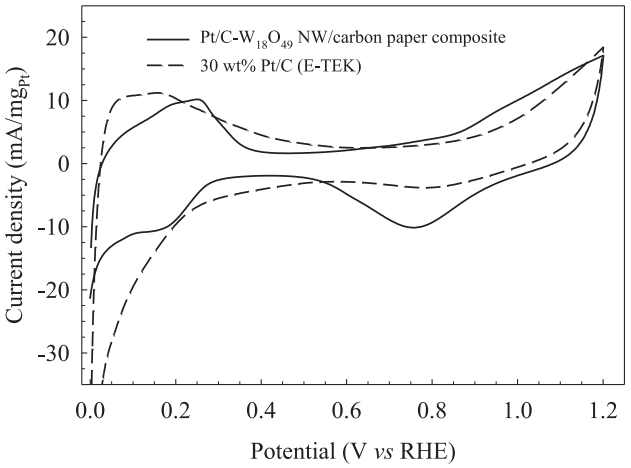

Fig. 4 – CVs of Pt/C–$W_{18}O_{49}$ NW/carbon paper composite and commercial Pt/C electrodes in 0.5 M H_2SO_4 aqueous solution at room temperature. Potential scan rate: 50 mV/s. Current densities normalized with respect to the Pt loading.

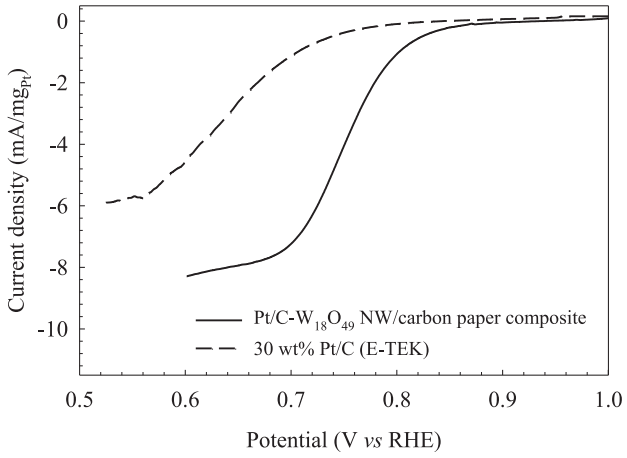

Fig. 5 – CVs for oxygen reduction reaction in O_2-saturated 0.5 M H_2SO_4 solution at different electrodes. Potential scan rate: 2 mV/s. Current densities normalized with respect to the Pt loading.

range and the reduction of Pt oxide at *ca.* +0.78 V. Characteristic peaks in the negative region (0.0–0.3 V) are attributed to atomic hydrogen adsorption on the Pt surface and reflect the electrochemical surface area of Pt. From the integrated charge in the hydrogen adsorption/desorption peak areas in the CV curves and the Pt poly-crystallite hydrogen adsorptions constant 0.21 mC/cm^2 Pt, the roughness factor (r_f, cm^2/cm$^2_{Pt}$) and the specific Pt surface areas (A_{Pt}, m^2/g$_{Pt}$) were calculated according to the following equations [39,40]:

$$r_f(\mathrm{cm}^2/\mathrm{cm}^2_{Pt}) = Q_M/0.21\ \mathrm{mC/cm}^2 \quad (1)$$

$$A_{Pt}(\mathrm{m}^2/\mathrm{g}_{Pt}) = r_f/[Pt] \quad (2)$$

where Q_M is the mean of charges exchanged during hydrogen adsorption and desorption (mC/cm^2), [Pt] is the platinum loading (mg/cm^2) on the electrode. The values of roughness factor and mass specific surface area are listed in Table 1. In the case of Pt/C–$W_{18}O_{49}$ NWs/carbon paper composite the roughness factor is significantly higher as compared to commercial Pt/C electrocatalysts (approximately 30%). The Pt/C–$W_{18}O_{49}$ NWs/carbon paper composite has the mass specific surface area (m^2/g$_{Pt}$, Table 1) of 63.5, about 36% higher than that of the commercial Pt/C electrode (40.6 m^2/g$_{Pt}$). This suggests that an increased Pt utilization of the Pt nanoparticles deposited onto C–$W_{18}O_{49}$ NWs/carbon paper that are in electrical contact with carbon paper.

The electrochemical performance of the Pt/C–$W_{18}O_{49}$ NWs/carbon paper electrode for oxygen reduction reaction was examined. The linear polarization curves are obtained from the linear scan voltammogram (LSV) shown in Fig. 5. For the oxygen reduction experiments at the Pt/C–$W_{18}O_{49}$ NWs/carbon paper and commercial Pt/C electrodes, a solution of 0.5 M H_2SO_4 was purged with ultrapure oxygen for 30 min, so that the solution becomes completely saturated with oxygen. These voltammograms reveal that the Pt/C–$W_{18}O_{49}$ NWs/carbon paper electrode is more active than Pt/C electrode. The onset potential for the oxygen reduction reaction is more positive potential for the Pt/C–$W_{18}O_{49}$ NWs/carbon paper composite (0.86 V vs. RHE) than the commercial Pt/C electrode (0.78 V). The half-wave potentials, $E_{1/2}$ of ORR of the Pt/C–$W_{18}O_{49}$ NWs/carbon paper composite is 0.75 V, also higher than 0.64 V for the reaction on commercial Pt/C electrode. The positive shift in the ORR onset and $E_{1/2}$ potentials indicates that the O_2 reduction reaction is more favorable on the Pt/C–$W_{18}O_{49}$ NWs/carbon paper composite than that on commercial Pt/C electrode. There are two ways to explain the activities of Pt-based electrocatalysts. One is mass activity (MA) associated with the current per amount

Table 1 – Characterization of Pt/C–$W_{18}O_{49}$ NWs/carbon paper and commercial 30 wt.% Pt/C electrodes.

Electrode	Pt loading (mg$_{Pt}$/cm^2)[a]	r_f(cm^2/cm$^2_{Pt}$)[b]	A_{Pt} (m^2/g$_{Pt}$)	Current density at 0.8 V	
				(mA/mg$_{Pt}$)[c]	(μA/cm$^2_{Pt}$)[d]
Pt/C–$W_{18}O_{49}$ NWs/carbon paper	0.18	114.3	63.5	0.83	1.3
30 wt.% Pt/C	0.20	81.2	40.6	0.20	0.5

a Measured by inductively coupled plasma-optical emission spectroscopy.
b r_f: real surface area obtained electrochemically from the hydrogen desorption regions of the voltammograms.
c Current normalized on the basis of Pt loading.
d Current normalized on the basis of real surface area of Pt.

of catalyst, and the other is specific activity (SA) related to the real surface area of platinum calculated from the hydrogen desorption regions of the CV. The MA (current normalized on the basis of Pt loading) and SA (current normalized on the basis of Pt surface area) at the potential of 0.8 V are also shown in Table 1. The Pt/C–$W_{18}O_{49}$ NWs/carbon paper composite showed a higher ORR current, and the MA is 0.83 mA/mg_{Pt}, which is 75% higher than the commercial Pt/C electrode, suggesting higher catalyst utilization for ORR. Further, it has also been shown that the SA of Pt/C–$W_{18}O_{49}$ NWs/carbon paper composite (1.3 $\mu A/cm^2_{Pt}$) is higher than the commercial Pt/C electrode (0.5 $\mu A/cm^2_{Pt}$). Based on the above results, it can be shown that the Pt/C–$W_{18}O_{49}$ NWs/carbon paper composite exhibits a better electrochemical activity for the oxygen reduction reaction as compared with that of the commercial Pt/C electrode. This improvement can be attributed to the higher dispersion of Pt nanoparticles on the surface of C–$W_{18}O_{49}$ NWs as well as the unique 3-D structure of Pt/C–$W_{18}O_{49}$ NWs/carbon paper composite. The catalysts made with Pt nanoparticles deposited onto C–$W_{18}O_{49}$ NWs exhibit a strong chemical interaction between Pt and $W_{18}O_{49}$ NWs surface, and this metal oxide-support interaction further improved the catalytic properties of the active metal through chemical effects. It has been reported that the catalysts made of Pt nanoparticles supported on WO_3 exhibit excellent CO tolerance and higher catalytic activity [29,30].

The durability of electrocatalyst has been recently recognized as one of the most important issues for fuel cells [41]. We also evaluated the durability of the Pt/C–$W_{18}O_{49}$ NWs/carbon paper electrode through repeated CV cycles with the appropriate lower and upper potential limits in an O_2-saturated 0.5 M H_2SO_4 solution. Fig. 6 shows the change of peak current density for oxygen reduction reaction with cycle number. The variation of the current density was only about 6% after 50 cycles, which implies that the Pt/C–$W_{18}O_{49}$ NWs/carbon paper electrode has a considerable stable electrocatalytic activity for oxygen reduction reaction.

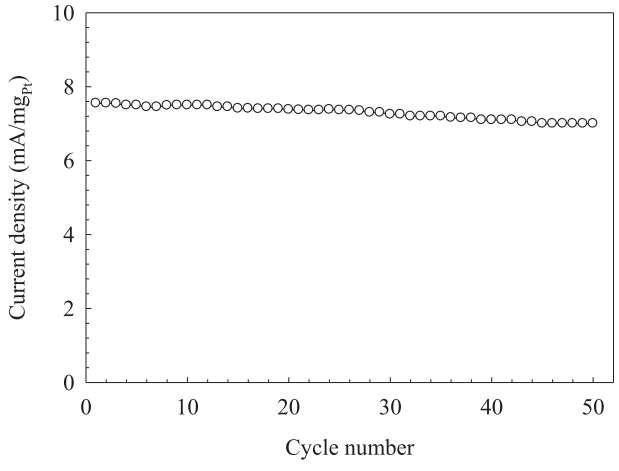

Fig. 6 – Stability of the Pt/C–$W_{18}O_{49}$ NW/carbon paper composite over 50 cycles of oxygen reduction reaction in O_2-saturated 0.5 M H_2SO_4 solution. Potential scan rate: 2 mV/s. Current densities normalized with respect to the Pt loading.

4. Conclusions

The composite electrodes of Pt/C–$W_{18}O_{49}$ NWs/carbon paper were prepared by growing C–$W_{18}O_{49}$ NWs directly on the carbon fibers of carbon paper by a thermal evaporation method, followed by the deposition of Pt nanoparticles onto NWs. TEM image shows that the Pt nanoparticles were uniformly dispersed with an average particle size of 2.27 nm. A 100 mV shift of the onset potential for oxygen reduction reaction at the Pt/C–$W_{18}O_{49}$ NWs/carbon paper electrode was observed as compared to Pt/C electrode. The Pt/C–$W_{18}O_{49}$ NWs/carbon paper composite electrode showed good stability and high catalytic activity for oxygen reduction reaction in acidic media, which could be attributed to the unique nanostructure of the composites: highly distributed Pt nanoparticles and high surface area of the support.

Acknowledgments

This research was supported by General Motors of Canada, Natural Sciences and Engineering Research Council of Canada (NSERC), Canada Foundation for Innovation (CFI), Ontario Early Researcher Award (ERA) and the University of Western Ontario (Academic Development Fund (ADF) and the Start-up Fund).

REFERENCES

[1] Gasteiger HA, Kocha SS, Sompalli B, Wagner FT. Activity benchmarks and requirements for Pt, Pt-alloy, and non-Pt oxygen reduction catalysts for PEMFCs. Appl Catal B Environ 2005;56:9–35.
[2] Williams MC, Strakey JP, Surdoval WA. The U.S. Department of Energy, Office of Fossil Energy stationary fuel cell program. J Power Sources 2005;143:191–6.
[3] Wang Y, Choi S, Lee E. Fuel cell power conditioning system design for residential application. Int J Hydrogen Energy 2009;34:2340–9.
[4] He T, Kreidler E, Xiong L, Luo J, Zhong CJ. Alloy electrocatalysts. J Electrochem Soc 2006;153:A1637–43.
[5] Freund A, Lang J, Lehmann T, Starz KA. Improved Pt alloy catalysts for fuel cells. Catal Today 1996;27:279–83.
[6] Ralph TR, Hogarth MP. Catalysis for low temperature fuel cells. Part I: the cathode challenges. Platin Met Rev 2002;46:3–14.
[7] Stevens DA, Dahn JR. Electrochemical characterization of the active surface in carbon-supported platinum electrocatalysts for PEM fuel cells. J Electrochem Soc 2003;150:A770–5.
[8] Liu L, Pu C, Viswanathan R, Fan Q, Liu R, Smotkin ES. Carbon supported and unsupported Pt–Ru anodes for liquid feed direct methanol fuel cells. Electrochim Acta 1998;43:3657–63.
[9] Litster S, McLean G. PEM fuel cell electrodes. J Power Sources 2004;130:61–76.
[10] Toda T, Igarashi H, Watanabe M. Role of electronic property of Pt and Pt alloys on electrocatalytic reduction of oxygen. J Electrochem Soc 1998;145:4185–8.
[11] Min M-K, Cho J, Cho K, Kim H. Particle size and alloying effects of Pt-based alloy catalysts for fuel cell applications. Electrochim Acta 2000;45:4211.

[12] Neergat N, Shukla AK, Gandhi KS. Platinum-based alloys as oxygen-reduction catalysts for solid-polymer-electrolyte direct methanol fuel cells. J Appl Electrochem 2001;31:373–8.
[13] Paffett MT, Berry JG, Gottesfeld S. Oxygen reduction at $Pt_{0.65}Cr_{0.35}$, $Pt_{0.2}Cr_{0.8}$ and roughened platinum. J Electrochem Soc 1988;135:1431–6.
[14] Toda T, Igarashi H, Watanabe M. Enhancement of the electrocatalytic O_2 reduction on Pt–Fe alloys. J Electroanal Chem 1999;460:258–62.
[15] Mukerjee S, Srinivasan S, Soriaga MP, McBreen J. Role of structural and electronic properties of Pt and Pt alloys on electrocatalysis of oxygen reduction. J Electrochem Soc 1995; 142:1409–22.
[16] Antolini E, Passos RR, Ticianelli EA. Electrocatalysis of oxygen reduction on a carbon supported platinum–vanadium alloy in polymer electrolyte fuel cells. Electrochim Acta 2002;48:263–70.
[17] Arico AS, Shukla AK, Kim H, Park S, Min M, Antonucci V. An XPS study on oxidation states of Pt and its alloys with Co and Cr and its relevance to electroreduction of oxygen. Appl Surf Sci 2001;172:33–40.
[18] Shukla AK, Neergat M, Bera P, Jayaram V, Hegde MS. An XPS study on binary and ternary alloys of transition metals with platinized carbon and its bearing upon oxygen electroreduction in direct methanol fuel cells. J Electroanal Chem 2001;504:111–9.
[19] Toda T, Igarashi H, Uchida H, Watanabe M. Enhancement of the electroreduction of oxygen on Pt alloys with Fe, Ni, and Co. J Electrochem Soc 1999;146:3750–6.
[20] Stamenkovic V, Schmidt TJ, Ross PN, Markovic NM. Surface composition effects in electrocatalysis: kinetics of oxygen reduction on well-defined Pt_3Ni and Pt_3Co alloy surfaces. J Phys Chem B 2002;106:11970–9.
[21] Kangasniemi KH, Condit DA, Jarvi TD. Characterization of Vulcan electrochemically oxidized under simulated PEM fuel cell conditions. J Electrochem Soc 2004;151:E125–32.
[22] Liu JG, Zhou ZH, Zhao XX, Xin Q, Sun GQ, Yi BL. Studies on performance degradation of a direct methanol fuel cell (DMFC) in life test. Phys Chem Chem Phys 2004;6:134–7.
[23] Borup R, Meyers J, Pivovar B, Kim YS, Mukundan R, Garland N, et al. Scientific aspects of polymer electrolyte fuel cell durability and degradation. Chem Rev 2007;107:3904–51.
[24] Lasch K, Jorrisen L, Garche J. The effect of metal oxides as co-catalysts for the electro-oxidation of methanol on platinum–ruthenium. J Power Sources 1999;84:225–30.
[25] McLeod EJ, Birss VI. Sol–gel derived WO_x and WO_x/Pt films for direct methanol fuel cell catalyst applications. Electrochim Acta 2005;51:684–93.
[26] Long WJ, Stroud MR, Swider-Lyons EK, Rolison RD. How to make electrocatalysts more active for direct methanol oxidation – avoid PtRu bimetallic alloys! J Phys Chem B 2000;104:9772–6.
[27] Shen PK, Tseung ACC. Anodic oxidation of methanol on Pt/WO_3 in acidic media. J Electrochem Soc 1994;141:3082–90.
[28] Gotz M, Wendt H. Binary and ternary anode catalyst formulations including the elements W, Sn and Mo for PEMFCs operated on methanol or reformate gas. Electrochim Acta 1998;43:3637–44.
[29] Jayaraman S, Jaramillo TF, Baeck S-H, McFarland EW. Synthesis and characterization of Pt–WO_3 as methanol oxidation catalysts for fuel cells. J Phys Chem B 2005;109:22958–66.
[30] Maillard F, Peyrelade E, Soldo-Olivier Y, Chatenet M, Chainet E, Faure R. Is carbon-supported Pt–WO_x composite a CO-tolerant material? Electrochim Acta 2006;52:1958–67.
[31] Savadogo O, Beck P. Five percent platinum–tungsten oxide-based electrocatalysts for phosphoric acid fuel cell cathodes. J Electrochem Soc 1996;143:3842–6.
[32] Wang ZL. Nanowires and nanobelts: materials, properties and devices. Boston, MA: Kluwer Academic; 2003.
[33] Saha MS, Li R, Cai M, Sun X. High electrocatalytic activity of platinum nanoparticles on SnO_2 nanowire-based electrodes. Electrochem Solid-State Lett 2007;10:B130–3.
[34] Saha MS, Li R, Sun X. Composite of Pt–Ru supported SnO_2 nanowires grown on carbon paper for electrocatalytic oxidation of methanol. Electrochem Commun 2007;9:2229–34.
[35] Saha MS, Banis MN, Zhang Y, Li R, Sun X, Cai M, et al. Tungsten oxide nanowires grown on carbon paper as Pt electrocatalyst support for high performance proton exchange membrane fuel cells. J Power Sources 2009;192:330–5.
[36] Saha MS, Li R, Sun X. High loading and monodispersed Pt nanoparticles on multiwalled carbon nanotubes for high performance proton exchange membrane fuel cells. J Power Sources 2008;177:314–22.
[37] Zhou Y, Zhang Y, Li R, Cai M, Sun X. One-step in situ synthesis and characterization of W18O49@carbon coaxial nanocables. J Mater Res 2009;24:1833–41.
[38] Bard AJ, Faulkner LR. Electrochemical methods, fundamentals and applications. New York: Wiley; 1980.
[39] Villers D, Sun SH, Serventi AM, Dodelet JP. Characterization of Pt nanoparticles deposited onto carbon nanotubes grown on carbon paper and evaluation of this electrode for the reduction of oxygen. J Phys Chem B 2006;110:25916–25.
[40] Woods R. Hydrogen adsorption on platinum, iridium and rhodium electrodes at reduced temperatures and the determination of real surface area. J Electroanal Chem Interfacial Electrochem 1974;49:217–26.
[41] Zhang J, Sasaki K, Sutter E, Adzic RR. Stabilization of platinum oxygen-reduction electrocatalysts using gold clusters. Science 2007;315:220–2.